NASA Technical Memorandum 102043
AIAA-89-2943

Average-Passage Simulation of Counter-Rotating Propfan Propulsion Systems as Applied to Cruise Missiles

Richard A. Mulac
Sverdrup Technology, Inc.
NASA Lewis Research Center Group
Cleveland, Ohio

Jon C. Schneider
McDonnell Douglas Astronautics Company
St. Louis, Missouri

and

John J. Adamczyk
National Aeronautics and Space Administration
Lewis Research Center
Cleveland, Ohio

Prepared for the
25th Joint Propulsion Conference
cosponsored by the AIAA, ASME, SAE, and ASEE
Monterey, California, July 10–12, 1989

NASA

AVERAGE-PASSAGE SIMULATION OF COUNTER-ROTATING PROPFAN PROPULSION SYSTEMS AS APPLIED TO CRUISE MISSILES

Richard A. Mulac*
Sverdrup Technology, Inc.
NASA Lewis Research Center Group
Cleveland, Ohio 44135

Jon C. Schneider†
McDonnell Douglas Astronautics Company
St. Louis, Missouri 63166

John J. Adamczyk‡
National Aeronautics and Space Administration
Lewis Research Center
Cleveland, Ohio 44135

Abstract

Counter-rotating propfan (CRP) propulsion technologies are currently being evaluated as cruise missile propulsion systems. The aerodynamic integration concerns associated with this application are being addressed through the computational modeling of the missile body - propfan flowfield interactions. The work described in this paper consists of a detailed analysis of the aerodynamic interactions between the control surfaces and the propfan blades through the solution of the average-passage equation system. Two baseline configurations were studied, the control fins mounted forward of the counter-rotating propeller and the control fins mounted aft of the counter-rotating propeller. In both cases, control fin - propfan separation distance and control fin deflection angle were varied.

Introduction

The maturation of missile propulsion systems has experienced a long and winding history. From the Wright's first powered flight in 1903 up through two World Wars, military applications of propeller propulsion systems had been applied solely to aircraft. Jet powered aircraft attaining higher speeds soon evolved, and with them came a desire for jet powered missiles. The German V-1 and American SNARK missiles are examples of these early attempts. Turbojet and turbofan powered missiles have since matured and developed into individual weapon systems such as the Harpoon and Tomahawk cruise missiles. With the growing desire for greater range capabilities from existing weapon systems, propeller propulsion systems may have presently found their place in missile system applications.

In order to maintain a strong defensive posture by providing the necessary range and an increased conventional payload delivery capability, more efficient cruise missile propulsion systems are needed. Propfan propulsion technologies have been shown to be capable of satisfying these requirements. Figure 1 shows a comparison of current and advanced turbofan and propfan engine performance, specific fuel consumption (SFC) versus thrust. For equivalent engine thrust levels and size, the propfan engine will be capable of providing greater range than its turbofan counterpart. Although the propfan engine has demonstrated its performance through the Douglas Aircraft Company Ultra-High Bypass engine program, much work must still be performed both analytically and experimentally to determine the operating capabilities of this propulsion system as applied to missiles.

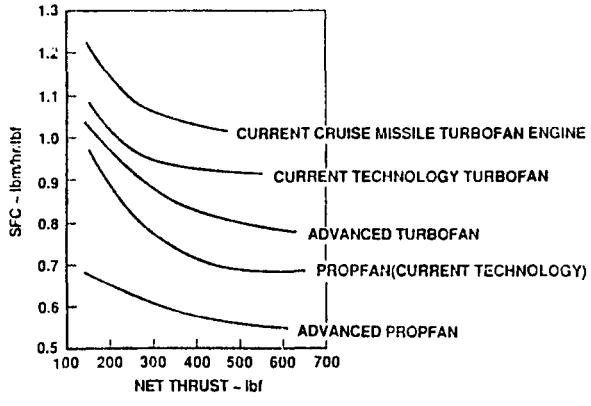

Figure 1.—Comparison of current and advanced engine performance.

* Programmer / Analyst, Member AIAA
† Engineer, Member AIAA
‡ Senior Research Scientist, Member AIAA

To date, the major effort in computational fluid dynamics as applied to propellers has been the development of efficient and accurate numerical procedures for solving the three-dimensional flow equations for a single propeller. These codes are based on either the inviscid or Reynolds-averaged form of the Navier-Stokes equations of motion, written with respect to an observer fixed in the frame of reference of the blade row. The inviscid codes have been extremely useful in identifying the three-dimensional shock structure within high-speed propellers. The viscous codes, because of the unavailability of sufficient computer capacity, have been limited to qualitative flow information. This, however, is changing rapidly as these codes become operational on supercomputers like the Cray Y-MP computer system with an SSD storage device or the Cray 2 computer system. The challenge currently facing propeller analysts is the extension of the three-dimensional isolated propeller codes to counter-rotating configurations.

A direct extension of either the three-dimensional inviscid or viscous isolated propeller codes noted previously to counter-rotating configurations would in general entail resolving the time-dependent flow field within each blade passage. For all but the simplest of configurations such an undertaking would be impractical for design applications, even on today's most advanced supercomputers. It is also by no means obvious that answers to many questions related to performance and durability require this degree of flow resolution.

An analysis was undertaken to develop a flow model describing the three-dimensional, deterministic, time-averaged flow field within a typical blade row passage of a multiple blade row configuration (ref. 1). The equations governing such a flow are referred to as the average-passage equation system. This flow model is a logical extension of the isolated blade row models. For multiple blade row configurations, the model describes the deterministic flow field within a blade passage as governed by the Reynolds-averaged form of the Navier-Stokes equations.

The average-passage equation system can be derived by first forming the ensemble average of the Navier-Stokes equations, which yield the familiar Reynolds-averaged form. Next the equations are time-averaged everywhere in space with respect to a frame of reference fixed to each blade row. Finally, the time-averaged flow field of each blade row is phase-lock averaged with respect to the tangential direction. This last operation yields a flow field that is spatially periodic from blade passage to blade passage within a given blade row. Through the average-passage model, each blade row is physically associated with a three-dimensional, time-averaged flow field that is periodic from blade passage to blade passage. One finds that these flow fields are coupled to one another through a system of body forces, energy sources, and momentum and energy correlations, all of which require some degree of empiricism to model. It is through these terms that the effects of neighboring blade rows on the flow field are introduced.

For simulations based on the inviscid form of the average-passage equation system, a closure model was developed (ref. 2) and incorporated into a computer program (SSTAGE) by Celestina and Adamczyk to solve the flow field associated with a single stage configuration. This code was successful in calculating the inviscid flow through a high-speed counter-rotating propeller (ref. 3). Their solution strategy consisted of a nested, two level, iterative procedure. The inner loop evaluated the three-dimensional flow variables for each blade row based on a distribution of body forces, energy sources, energy correlations, and velocity correlations which accounted for the presence of the neighboring blade row. This was performed using a four stage Runge-Kutta integration procedure (ref. 4), which converged each flow field solution to within a specified tolerance. Upon convergence of all blade row solutions, the axisymmetric average of each blade row's three-dimensional flow field was evaluated. The outer loop then evaluated the discrepancy between the axisymmetric solutions. According to the closure model, each blade row's axisymmetric solution should converge to a single common axisymmetric solution (within a limit set by the computational mesh size). If the difference between the axisymmetric solutions was greater than a set tolerance, the body forces, energy sources, energy correlations, and velocity correlations were recalculated for each blade row based on their respective estimated average-passage solution. The inner loop was then repeated using the updated information. When the outer loop convergence criteria was eventually met, the numerical simulation was complete.

The individual blade row flow calculations within the inner loop are completely independent, making them very amenable to parallel processing. Mulac, Celestina, and Adamczyk applied multitasking and an out-of-core data structure to the inviscid form of the average-passage equation system and created a program (MSTAGE) which allowed for the numerical simulation of multiple stage configurations. This code was successful in calculating the inviscid flow through a two stage, axial flow turbine (ref. 5).

Average-Passage Model

The three-dimensional average-passage equation system for a multiple blade row configuration can be

written in cylindrical (z, r, θ) coordinates as

$$\int (\lambda u_t) dVol + L(\lambda u) + \int \lambda S dVol = \int \lambda K dVol \quad (1)$$

The vector u contains the flow variables density, axial, radial, and angular momenta, and total internal energy. The variable λ is the neighboring blade row's blockage attributed to their thickness. The value of this parameter ranges between zero and unity, unity being the value associated with a blade of zero thickness. The operator $L(\lambda u)$ balances the mass, axial, radial, and angular momenta, and energy through a control volume. $\int \lambda S dVol$ contains the body forces, energy sources, and energy and velocity correlations associated with the neighboring blade rows, while $\int \lambda K dVol$ is a source term due to the cylindrical coordinate system.

The solution to equation (1) is obtained for each blade row using appropriate boundary conditions and fixing the body forces from the neighboring blade rows. A Runge-Kutta scheme (ref. 4) is used to drive the time derivative to below some specified tolerance. Stability is maintained using a blend of second and fourth difference smoothing operators. Convergence accelerators such as local time stepping and implicit residual averaging are also used. Solving equation (1) independently for each blade row is considered the inner loop. When each cycle of the inner loop is completed, the axisymmetric solution and body forces are updated for each blade row and the inner loop procedure is repeated. This repitition of the inner loop procedure is considered the outer loop. When the axisymmetric average of each blade row's solution has converged to a single axisymmetric solution for all blade rows, the simulation is complete. Further information on the average-passage equation system and its implementation can be found in references 1, 2, 3, and 5.

The present solution algorithm requires each blade row to have its own unique computational H-mesh describing its respective passage. However, all meshes must share common axial and radial coordinates as shown in figure 2. This eliminates the need to interpolate the flow variables between the individual flow field calculations. A mesh generator satisfying these criteria (ref. 6) is used to create the meshes required by the solution algorithm. The axisymmetric view of the mesh shown in figure 2 is that of the control fin forward propfan powered cruise missile configuration. The mid-channel view of the control fin, forward propeller, and aft propeller meshes is shown in figures 3, 4, and 5, respectively.

The inner loop procedure previously described calculates each blade row's flow field solution independently. This makes it an ideal candidate for parallel processing (ref. 5). Each blade row has its own set of

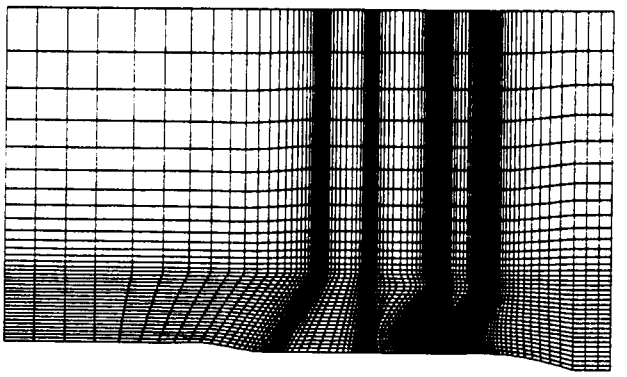

Figure 2.—Common axisymmetric mesh.

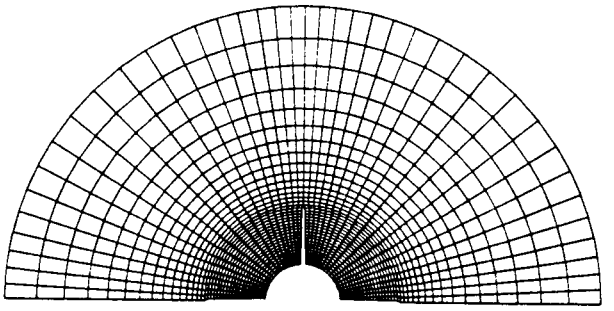

Figure 3.—Mid-channel view of the control fin mesh.

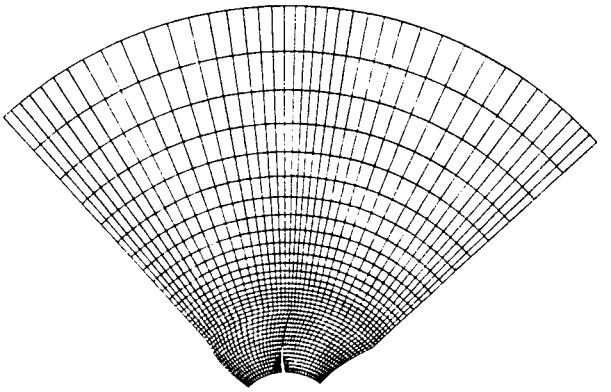

Figure 4.—Mid-channel view of the forward propeller mesh.

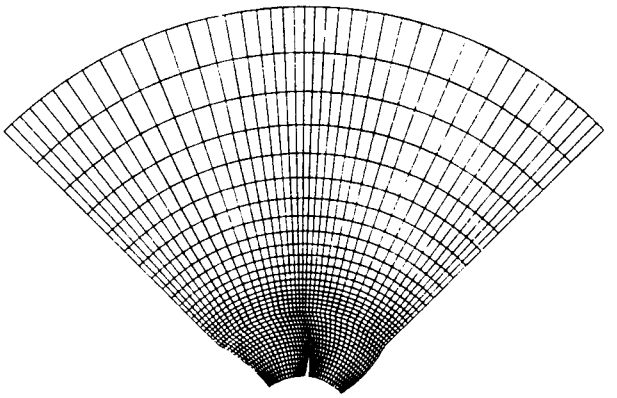

Figure 5.—Mid-channel view of the aft propeller mesh.

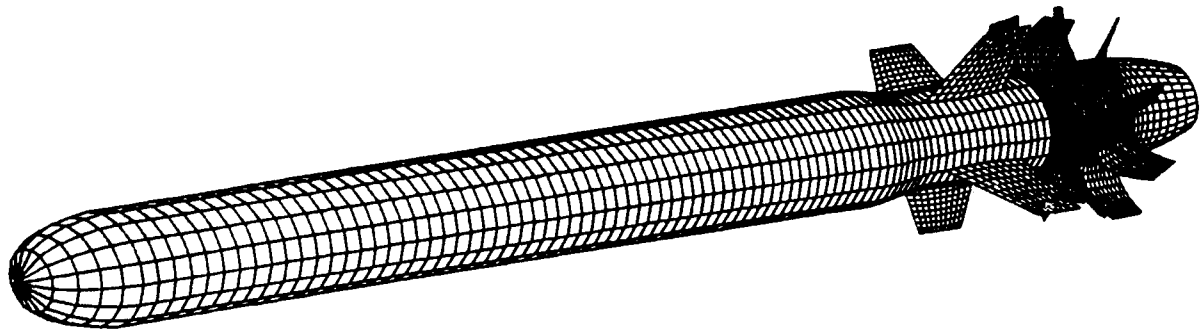

Figure 6.—Propfan powered cruise missile.

flow variables and a unique computational mesh. The only time data is shared between the individual flow field calculations is immediately before entering the inner loop. Because of this independence, an N blade row simulation running on a dedicated N processor computer should use approximately the same wall clock time as a single blade row simulation since over ninety-seven percent of the computational work required for the simulation is performed within the inner loop.

The storage problem associated with the solution algorithm is solved by taking the three-dimensional mesh and flow field quantities and storing them as a series of two-dimensional arrays stacked upon one another (ref. 5). In this way only the planes of data which are currently required by the solution procedure would have to lie in main memory, at other times they could remain out on secondary storage in a random access file.

Propfan Powered Cruise Missile Application

The arena for application of propfan propulsion technologies lies in intermediate and long range cruise missile missions. As previously mentioned, propfan propulsion technology has been shown to be capable of providing performance (SFC) improvements over conventional turbofan propulsion systems. These performance improvements can also be realized in missile size and weight reductions for fixed range missions. Therefore, vehicles currently configured could be modified with a propfan propulsion system as shown in figure 6 for two purposes; to maintain range while reducing vehicle size and weight, and to maintain vehicle size and weight while increasing range.

For cruise missile applications, there are two baseline candidate configurations and associated with each are several pros and cons. The first configuration consists of the control fins mounted forward of the counter-rotating propeller. The advantage of this method is in the ease of structural integration into the missile. The potential disadvantages include blade structural fatigue due to the varying incidence angle induced by the control fins and the decrease of vehicle controlability due to the control fins being positioned closer to the missile's center of gravity. The second configuration consists of the control fins mounted aft of the counter-rotating propeller. This provides for greater control due to the control fins being positioned further from the missile's center of gravity and the accelerated flow they receive from the counter-rotating propeller. The structural integration of this design is difficult though, due to the increased loading on the aft section of the missile by the control fins.

The MSTAGE code was used to simulate both the control fin forward and control fin aft configurations under several permuted flight conditions. Figures 7 and 8 show a three-dimensional view representing the configurations with the control fins located forward and aft of the propfan blades, respectively. In the two

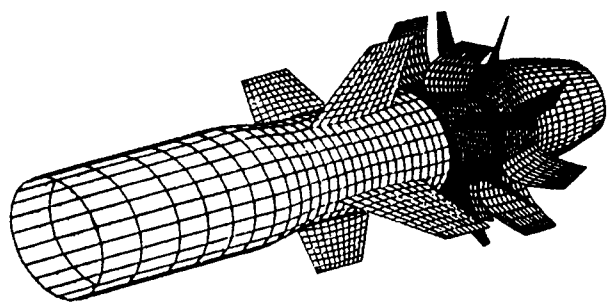

Figure 7.—Control fin forward configuration.

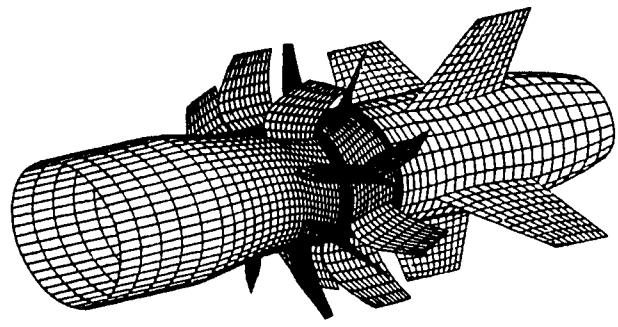

Figure 8.—Control fin aft configuration.

configurations, the control fin - propfan separation was set at both 0.25 and 0.5 control fin root chords and the control fin deflection angle was varied from −15 to +15 degrees. The operating condition for the cruise missile was fixed for the entire set of simulations. This particular cruise missile was designed to fly at a Mach number of 0.7 at sea level with the advance ratios of the forward and aft propellers set at +2.78 and −2.78, respectively.

The solution to the average-passage equation system for the propfan powered cruise missile gives a description of the flow field associated with a configuration in which all the control fins have identical deflection angles. In reality, the top, left, and right control fins are capable of independently varying their angle of attack, while the bottom control fin is in a fixed position. A significant amount of both computer time and memory would be required to simulate the entire range of control fin permutations which occur during flight. The study presented here, consisting of a wide range of control fin deflection angle settings, should give design engineers valuable insight into the performance trends of various configurations, allowing them to screen new candidate configurations in the early stages of developement.

Results

As mentioned previously, two baseline configurations were studied; the control fins located forward of the propfan blades, and the control fins located aft of the propfan blades. The control fin blade row contained four blades, while the propfan blade rows each contained eight blades. Several perturbations were made to each of the baseline configurations. The control fin - propfan separation was set at both 0.25 and 0.5 control fin root chords and the control fin deflection angle was varied from −15 to +15 degrees. The sign convention used with respect to the control fin deflection angle is based on the following frame of reference. With the missile in a position such that the flow is moving from left to right, if the leading edge of the control fin is lower than the trailing edge, the deflection angle is negative. If the leading edge of the control fin is higher than the trailing edge, the deflection angle is positive.

A total of twenty simulations were performed using a Cray X-MP/24 (2 processors, 4 million word memory) supercomputer with an accompanying 64 million word SSD. A summary of the simulations is available in figure 9. Each mesh used in the simulations had a dimension of 36 in the radial direction and 21 in the circumferen-

CONTROL FIN FORWARD CONFIGURATIONS			
Case	Mesh Size	Fin Angle	Fin–Prop Separation
1	139 x 36 x 21	−15°	1/2 fin chord
2	139 x 36 x 21	−10°	1/2 fin chord
3	139 x 36 x 21	−5°	1/2 fin chord
4	139 x 36 x 21	−3°	1/2 fin chord
5	139 x 36 x 21	0°	1/2 fin chord
6	139 x 36 x 21	+3°	1/2 fin chord
7	139 x 36 x 21	+5°	1/2 fin chord
8	139 x 36 x 21	+10°	1/2 fin chord
9	139 x 36 x 21	+15°	1/2 fin chord
10	135 x 36 x 21	−5°	1/4 fin chord
11	135 x 36 x 21	−3°	1/4 fin chord
12	135 x 36 x 21	0°	1/4 fin chord
CONTROL FIN AFT CONFIGURATIONS			
Case	Mesh Size	Fin Angle	Fin–Prop Separation
13	141 x 36 x 21	−15°	1/2 fin chord
14	141 x 36 x 21	−10°	1/2 fin chord
15	141 x 36 x 21	−5°	1/2 fin chord
16	141 x 36 x 21	−3°	1/2 fin chord
17	141 x 36 x 21	0°	1/2 fin chord
18	139 x 36 x 21	−5°	1/4 fin chord
19	139 x 36 x 21	−3°	1/4 fin chord
20	139 x 36 x 21	0°	1/4 fin chord

Figure 9.—Propfan powered cruise missile simulation summary.

tial direction, while the axial dimension varied from 135 to 141. The control fin was defined by 21 points axially and 21 points radially. Each of the counter-rotating propeller blades was defined by 21 points axially and 16 points radially. Mesh points were packed at the leading and trailing edges of the control fin and propfan blades. 2.8 million words of main memory and 23 million words of SSD storage were required for each simulation.

Each of the twenty simulations required between four and seven iterations (swaps) of the outer loop procedure in order to obtain a converged solution. Each iteration of the outer loop consisted of three iterations of the inner loop procedure, one for each blade row. Each iteration of the inner loop procedure performed 750 iterations of the Runge-Kutta integration scheme on its respective blade row solution. The average CPU time required for each iteration of the Runge-Kutta scheme was 2.25 seconds, leading to each iteration of the outer loop procedure consuming approximately 1.5 hours. The CPU time thus consumed by each of the twenty simulations varied from a minimum of 6 hours to a maximum of 10.5 hours.

The convergence history of case 7 is representative of that obtained for all twenty simulations. The configuration consisted of the control fin set forward of the propfan at a separation of 0.5 control fin root chords, with a deflection angle of +5 degrees. Figure 10 shows the convergence rate of the axisymmetric solutions associated with each of the three blade rows of case 7. The L_2 norm of the residual plotted in figure 10 is the difference between the axisymmetric components of all blade row pair combinations at each iteration of the outer loop (swap). After six swaps, the L_2 norm of the residual approached an asymptotic limit indicating that the simulation was complete.

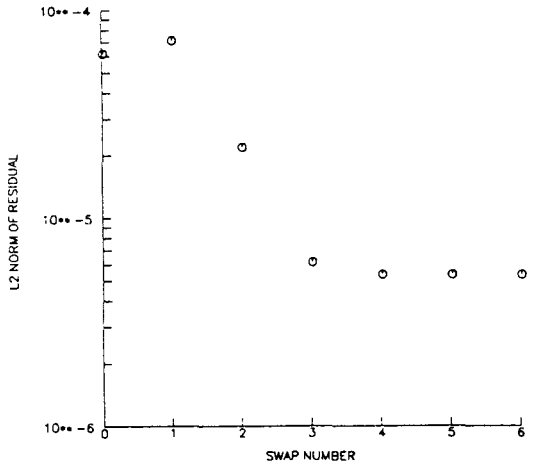

Figure 10.—Outer loop convergence.

A comparison of the convergence history of the inner loop procedure for case 7 is made in figures 11 and 12. The L_2 norms of the individual solution residuals have dropped over two orders of magnitude by the sixth swap of the outer loop procedure as compared to the initial swap. The residual limit of 10^{-6} reached by the control fin solution at the sixth swap is due to a vortex which formed at the control fin tip. Three-dimensional structures such as this tend to limit the convergence level of the solution to the average-passage equation system.

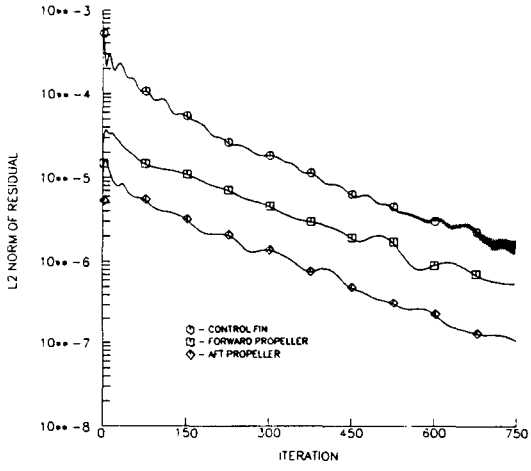

Figure 11.—Inner loop convergence (zeroth swap).

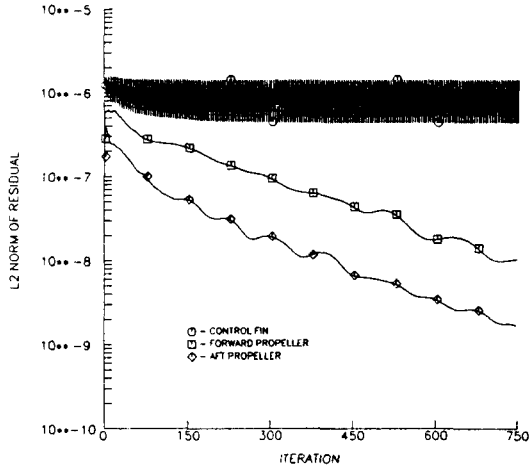

Figure 12.—Inner loop convergence (sixth swap).

In each of the twenty cases, both the thrust coefficient and power coefficient associated with the propfan were calculated by integrating the pressure distribution across each propeller. At the time of publication of this

paper, no experimental data was available to the authors on either of the candidate configurations. Thrust and power coefficient associated with the forward propeller versus control fin deflection angle is shown in figures 13 and 14, respectively. Regarding the control fin forward configurations (cases 1 – 12), it is evident that as the control fin deflection angle decreases negatively, the thrust and power coefficients become negative. This is due to the decreased incidence angle to the forward propeller, causing the propeller to absorb energy from the flow and act as a turbine. As the control fin deflection angle increases positively, the incidence increases causing both the thrust and power to increase.

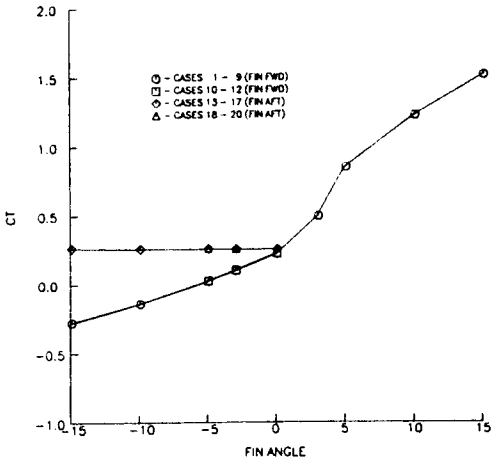

Figure 13.—Thrust coefficient versus fin angle (forward propeller).

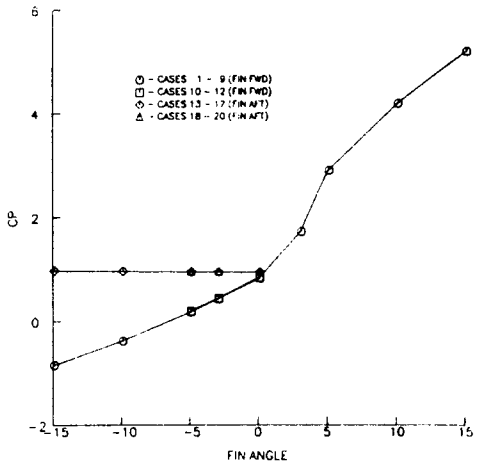

Figure 14.—Power coefficient versus fin angle (forward propeller).

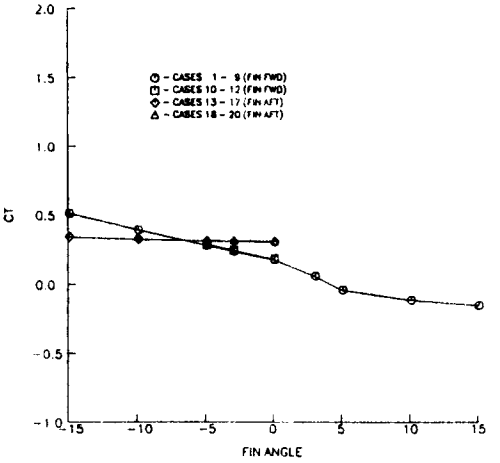

Figure 15.—Thrust coefficient versus fin angle (aft propeller).

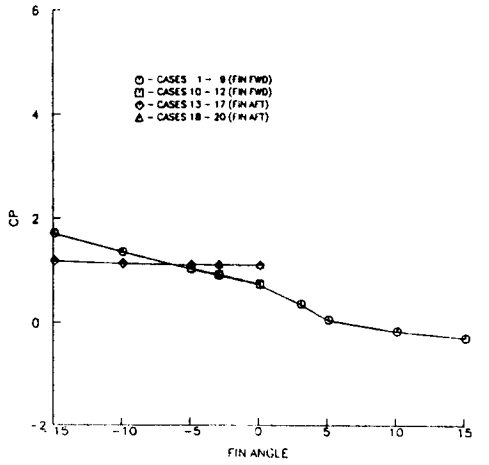

Figure 16.—Power coefficient versus fin angle (aft propeller).

The effect of varying the control fin deflection angle on the thrust and power coefficient of the aft propeller is shown in figures 15 and 16, respectively. With the aft propeller rotating in the opposite direction of the forward propeller, the variation of the thrust and power coefficient is the reverse of that seen for the forward propeller, although the magnitude of the variation is not as pronounced.

The influence of the control fin deflection angle on the thrust and power coefficient for the counter-rotating system is shown in figures 17 and 18, respectively. Here the system thrust or power coefficient is simply the sum

of the forward and aft propeller coefficients. Again, for the control fin forward configurations (cases 1 – 12), it is evident that as the control fin deflection angle decreases negatively, the thrust and power coefficients become negative. As the control fin deflection angle increases positively, both thrust and power increase accordingly. Thrust and power coefficients remained nearly constant for the control fin aft configurations (cases 13 – 20), showing little change with respect to the control fin deflection angle. For this reason it was deemed unnecessary to simulate the control fin aft configuration for positive control fin deflection angles.

According to the inviscid average-passage model, if there is no significant radial change in the path of a fluid particle departing from either the control fin in the control fin forward configuration or the propeller in the control fin aft configuration, a change in the control fin - propfan separation distance will have little effect on the resultant flow field. This can be seen in figures 17 and 18 for the control fin forward configuration (cases 10–12) and for the control fin aft configuration (cases 18–20). Because little effect was seen in changing the control fin - propeller separation distance, this parameter was varied the least.

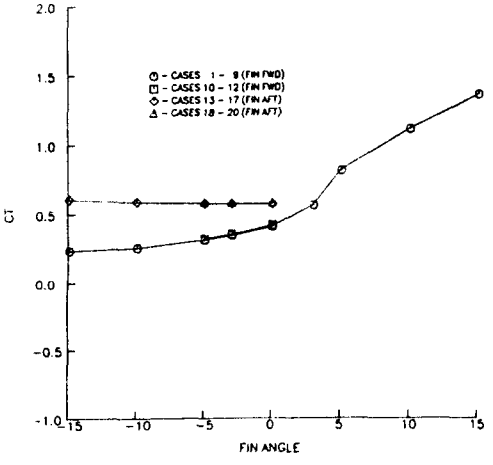

Figure 17.—Thrust coefficient versus fin angle (counter-rotating system).

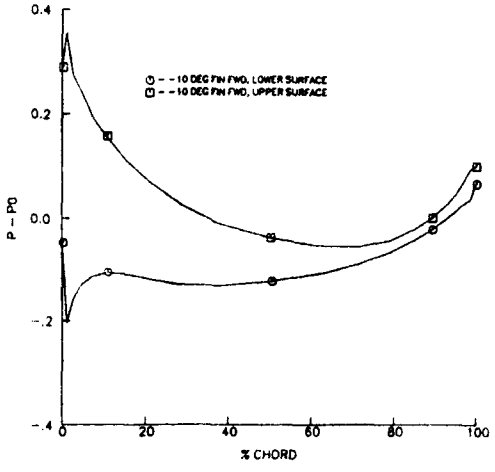

Figure 19.—Control fin forward pressure distribution (−10° deflection angle).

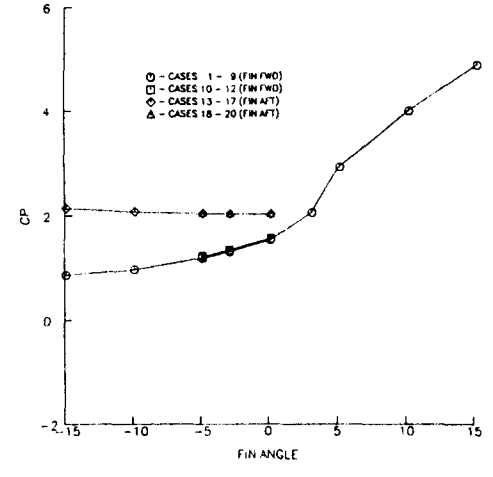

Figure 18.—Power coefficient versus fin angle (counter-rotating system).

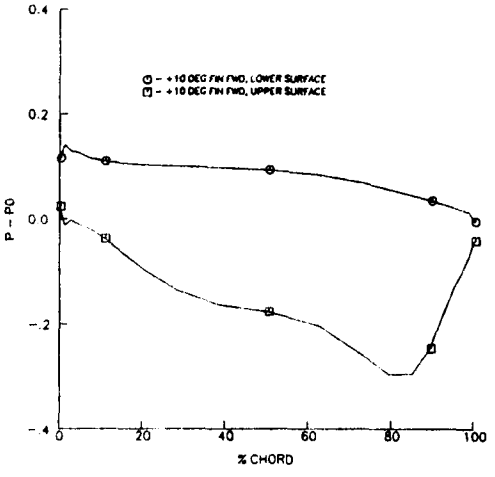

Figure 20.—Control fin forward pressure distribution (+10° deflection angle).

To further analyze the effect of negative or positive control fin deflection angles on the control fin forward configuration, the pressure distribution along the control fin near the hub was analyzed. Figure 19 shows the pressure distribution along the control fin at a −10 degree deflection. As was previously stated, the counter-rotating propeller was shown to have absorbed energy from the flow in this situation, causing the flow across the control fin to decrease. The pressure distribution shown in figure 19 is typical of that seen in the case of subsonic flow over an airfoil. Figure 20 shows the pressure distribution along the control fin at a +10 degree deflection. In this case the thrust produced by the counter-rotating propeller increased, causing the flow across the control fin to increase. The pressure distribution shown in figure 20 is typical of that seen in the case of transonic flow over an airfoil.

Figures 21 and 22 show the pressure distribution along the suction and pressure surfaces of the forward propeller near the hub for the control fin aft configuration at a 0 degree deflection and the control fin forward configuration at both −10 and +10 degree deflection. Using the 0 degree deflection control fin aft configuration as a reference, the unloading of the propeller blade is seen in the case of the control fin forward configuration at a −10 degree deflection, while the increased loading of the propeller is apparent at a +10 degree deflection.

Normalized control fin loading is plotted against the control fin deflection angle in figure 23. The control fin loading for all twenty cases was normalized by the loading on the +15 degree deflection control fin forward configuration. For identical control fin deflection angles ranging from 0 to −15 degrees, the control fin loading of the control fin aft configuration is greater than its control fin forward counterpart, becoming more pronounced as the deflection angle decreases negatively. The reason for this behavior can be explained by examining the pressure distribution along the control fin at both 0 and −10 degrees of deflection. The pressure distribution near the hub of the 0 and −10 degree deflection control fin for the control fin forward and aft configurations is shown in figures 24 and 25, respectively. The difference between the control fin forward and the control fin aft pressure distribution is due to the counter-rotating propeller accelerating the flow, which accounts for the increased loading in the control fin aft configurations.

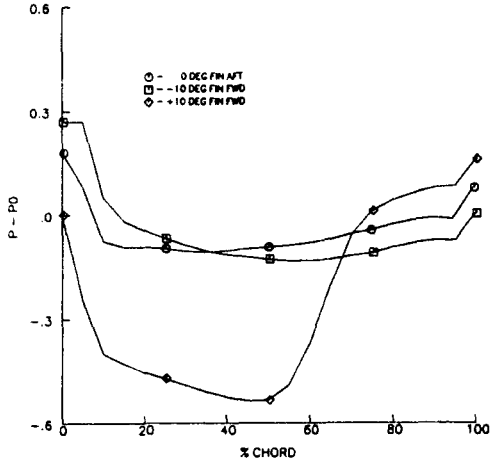

Figure 21.—Forward propeller suction surface pressure distribution.

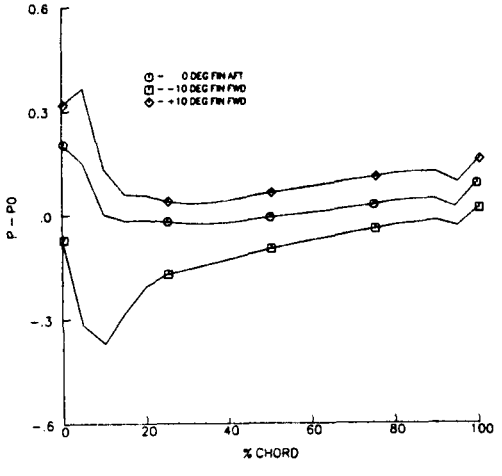

Figure 22.—Forward propeller pressure surface pressure distribution.

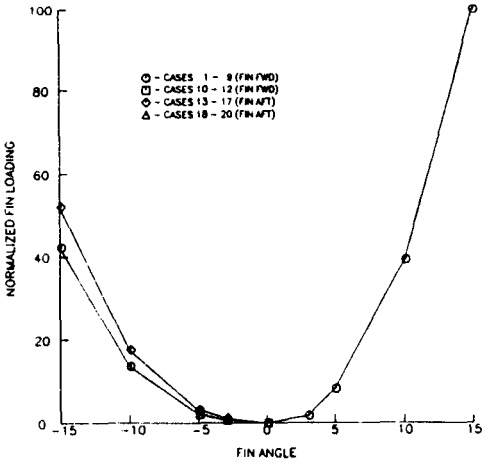

Figure 23.—Normalized fin loading versus fin angle.

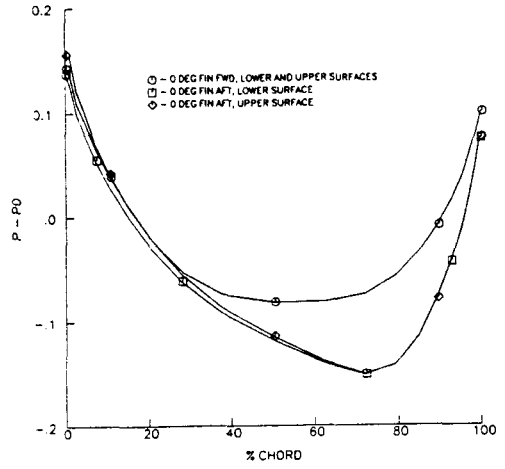

Figure 24.—Control fin forward and aft pressure distribution (0° deflection angle).

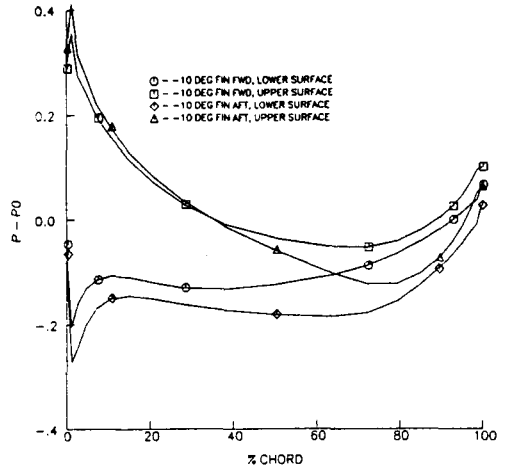

Figure 25.—Control fin forward and aft pressure distribution (−10° deflection angle).

Conclusions

Several candidate configurations of a propfan powered cruise missile were successfully simulated through the solution of the average-passage equation system. An analysis of the results led to a number of conclusions. It appeared that it is desirable to locate low aspect ratio control surfaces aft of a counter-rotating propfan, as opposed to mounting the control fins forward of the propfan. Simulations such as those described herein should reduce the size of a control fin deflection angle experimental matrix by focusing in on the extreme fin deflection angle settings. Because the simulations were inviscid, though, the effect of control fin - propfan seperation should be analyzed further. Insight was also provided into the loading variation of the propfan blades located behind a deflected control surface through one revolution.

Acknowledgment

The authors wish to thank Georges Pechuzal, K.C. Bush, and Brian Sill of the Garrett Turbine Engine Company and Chris Thornton of the McDonnell Douglas Astronautics Company for their help in supplying the geometry and operating condition for the propfan powered cruise missile. Thanks also to Chris Miller of the Propulsion Systems Division at the NASA Lewis Research Center and Mark Celestina of Sverdrup Technology's Lewis Research Center Group for their help in analyzing the performance of the various configurations simulated.

References

1. Adamczyk, J.J., "Model Equation for Simulating Flows in Multistage Turbomachinery," NASA TM-86869, ASME Paper No. 85-GT-226, Nov. 1984.
2. Adamczyk, J.J., Mulac, R.A., and Celestina, M.L., "A Model for Closing the Inviscid Form of the Average-Passage Equation System," NASA TM-87199, ASME Paper 86-GT-227, June 1986.
3. Celestina, M.L., Mulac, R.A., and Adamczyk, J.J., "A Numerical Simulation of the Inviscid Flow Through a Counter-Rotating Propeller," NASA TM-87200, ASME Paper 86-GT-138, June 1986.
4. Jameson, A., Schmidt, W., and Turkel, E., "Numerical Solutions of the Euler Equations by Finite Volume Methods Using Runge-Kutta Time-Stepping Schemes," AIAA-81-1259, June 1981.
5. Mulac, R.A., Celestina, M.L., Adamczyk, J.J., Misegades, K.P., and Dawson, J.M., "The Utilization of Parallel Processing in Solving the Inviscid Form of the Average-Passage Equation System for Multistage Turbomachinery," NASA TM-89845, AIAA Paper 87-1197, June 1987.
6. Mulac, R.A., "A Multistage Mesh Generator for Solving the Average-Passage Equation System," NASA CR-179539, Jan. 1988.

NASA
National Aeronautics and Space Administration

Report Documentation Page

1. Report No.	2. Government Accession No.	3. Recipient's Catalog No.
NASA TM-102043 AIAA-89-2943		

4. Title and Subtitle

Average-Passage Simulation of Counter-Rotating Propfan Propulsion Systems as Applied to Cruise Missiles

5. Report Date

6. Performing Organization Code

7. Author(s)

Richard A. Mulac, Jon C. Schneider, and John J. Adamczyk

8. Performing Organization Report No.

E-4791

10. Work Unit No.

505-90-01

9. Performing Organization Name and Address

National Aeronautics and Space Administration
Lewis Research Center
Cleveland, Ohio 44135-3191

11. Contract or Grant No.

13. Type of Report and Period Covered

Technical Memorandum

12. Sponsoring Agency Name and Address

National Aeronautics and Space Administration
Washington, D.C. 20546-0001

14. Sponsoring Agency Code

15. Supplementary Notes

Prepared for the 25th Joint Propulsion Conference cosponsored by the AIAA, ASME, SAE, and ASEE, Monterey, California, July 10-12, 1989. Richard A. Mulac, Sverdrup Technology, Inc., NASA Lewis Research Center Group, Cleveland, Ohio 44135; Jon C. Schneider, McDonnell Douglas Astronautics Company, St. Louis, Missouri 63166; John J. Adamczyk, NASA Lewis Research Center.

16. Abstract

Counter-rotating propfan (CRP) propulsion technologies are currently being evaluated as cruise missile propulsion systems. The aerodynamic integration concerns associated with this application are being addressed through the computational modeling of the missile body—propfan flowfield interactions. The work described in this paper consists of a detailed analysis of the aerodynamic interactions between the control surfaces and the propfan blades through the solution of the average-passage equation system. Two baseline configurations were studied, the control fins mounted forward of the counter-rotating propeller and the control fins mounted aft of the counter-rotating propeller. In both cases, control fin—propfan separation distance and control fin deflection angle were varied.

17. Key Words (Suggested by Author(s))	18. Distribution Statement
Average-passage Propfan Cruise missile	Unclassified – Unlimited Subject Category 02

19. Security Classif. (of this report)	20. Security Classif. (of this page)	21. No of pages	22. Price*
Unclassified	Unclassified	12	A03

NASA FORM 1626 OCT 86

*For sale by the National Technical Information Service, Springfield, Virginia 22161